



## Article

# Simulation of Dissipative Hybrid Nanofluid (PEG-Water + $ZrO_2$ + $MgO$ ) Flow by a Curved Shrinking Sheet with Thermal Radiation and Higher Order Chemical Reaction

Gopinath Veeram <sup>1,†</sup>, Pasam Poojitha <sup>1</sup>, Harika Katta <sup>1</sup>, Sanakkayala Hemalatha <sup>2</sup>, Macherla Jayachandra Babu <sup>3</sup>, Chakravarthula S. K. Raju <sup>4</sup>, Nehad Ali Shah <sup>5,†</sup> and Se-Jin Yook <sup>4,\*</sup>

<sup>1</sup> Department of Mathematics, Chinthalapati Satyavathi Devi St. Theresa's College for Women (A), Eluru 534003, Andhra Pradesh, India; gopinath.veeram@stcelr.ac.in (G.V.); poojithapasam@stcelr.ac.in (P.P.); harika.katta@stcelr.ac.in (H.K.)

<sup>2</sup> Department of Mathematics, Sir Cattamanchi Ramalinga Reddy College, Eluru 534007, Andhra Pradesh, India; shl@sircreddycollege.ac.in

<sup>3</sup> Department of Mathematics, Swamy Vidyaprakasanaanda Government College, Srikalahasti 517644, Andhra Pradesh, India; mjayachandra@svagovtcm.ac.in

<sup>4</sup> School of Mechanical Engineering, Hanyang University, 222 Wangsimni-ro, Seongdong-gu, Seoul 04763, Korea; rchakrav@gitam.edu

<sup>5</sup> Department of Mechanical Engineering, Sejong University, Seoul 05006, Korea; nehadali199@sejong.ac.kr

\* Correspondence: ysjnuri@hanyang.ac.kr

† These authors contributed equally to this work and are co-first authors.



**Citation:** Veeram, G.; Poojitha, P.; Katta, H.; Hemalatha, S.; Babu, M.J.; Raju, C.S.K.; Shah, N.A.; Yook, S.-J. Simulation of Dissipative Hybrid Nanofluid (PEG-Water +  $ZrO_2$  +  $MgO$ ) Flow by a Curved Shrinking Sheet with Thermal Radiation and Higher Order Chemical Reaction. *Mathematics* **2022**, *10*, 1706. <https://doi.org/10.3390/math10101706>

Academic Editor: Carlos Llopis-Albert

Received: 4 April 2022

Accepted: 12 May 2022

Published: 16 May 2022

**Publisher's Note:** MDPI stays neutral with regard to jurisdictional claims in published maps and institutional affiliations.



**Copyright:** © 2022 by the authors. Licensee MDPI, Basel, Switzerland. This article is an open access article distributed under the terms and conditions of the Creative Commons Attribution (CC BY) license (<https://creativecommons.org/licenses/by/4.0/>).

**Abstract:** The heat transmission capabilities of hybrid nanofluids are superior to those of mono nanofluids. In addition to solar collectors and military equipment, they may be found in a number of areas including heat exchanger, automotive industry, transformer cooling and electronic cooling. The purpose of this study was to evaluate the significance of the higher order chemical reaction parameter on the radiative flow of hybrid nanofluid (polyethylene glycol (PEG)–water combination: base fluid and zirconium dioxide, magnesium oxide: nanoparticles) via a curved shrinking sheet with viscous dissipation. Flow-driven equations were transformed into nonlinear ODEs using appropriate similarity transmutations, and then solved using the *bvp4c* solver (MATLAB built-in function). The results of two scenarios, *PEG – Water +  $ZrO_2$  +  $MgO$*  (hybrid nanofluid) and *PEG – Water +  $ZrO_2$* , (nanofluid) are reported. In order to draw important inferences about physical features, such as heat transfer rate, a correlation coefficient was used. The main findings of this study were that curvature parameter lowers fluid velocity, and Eckert number increases the temperature of fluid. It was observed that the volume fraction of nanoparticles enhances the skin friction coefficient and curvature parameter lessens the same. It was noticed that when curvature parameter ( $K$ ) takes input in the range  $0.5 \leq K \leq 2.5$ , the skin friction coefficient decreases at a rate of 1.46633 (i.e., 146.633%) (in the case of hybrid nanofluid) and 1.11236 (i.e., 111.236%) (in the case of nanofluid) per unit value of curvature parameter. Increasing rates in the skin friction parameter were 3.481179 (i.e., 348.1179%) (in the case of hybrid nanofluid) and 2.745679 (in the case of nanofluid) when the volume fraction of nanoparticle ( $\phi_1$ ) takes input in the range  $0 \leq \phi_1 \leq 0.2$ . It was detected that, when Eckert number ( $E_{ck}$ ) increases, Nusselt number decreases. The decrement rates were observed as 1.41148 (i.e., 141.148%) (in the case of hybrid nanofluid) and 1.15337 (i.e., 153.337%) (in the case of nanofluid) when Eckert number takes input in the range  $0 \leq E_{ck} \leq 0.2$ . In case of hybrid nanofluid, it was discovered that the mass transfer rate increases at a rate of 1.497214 (i.e., 149.7214%) when chemical reaction ( $Kr$ ) takes input in the range  $0 \leq Kr \leq 0.2$ . In addition, we checked our findings against those of other researchers and discovered a respectable degree of agreement.

**Keywords:** hybrid nanofluid; curved shrinking sheet; thermal radiation; Eckert number; correlation coefficient; chemical reaction

**MSC:** 74A30; 74A65

## 1. Introduction

Thermal radiation involves the flow of internal energy in the form of electromagnetic waves. Radiation has a substantial effect on flow during processes involving high temperatures, such as the production of proper plates. Ibrahim and Hady [1] used Rosseland approximation to depict the radiative heat flux (in the energy equation) in the scrutiny of laminar plane flow, and obtained that the thermal radiation increases the convective flow. A decrease in velocity was shown to be associated with increasing porosity, according to Bhatti et al. [2]. Squeezing nanofluid between two parallel plates with the radiation parameter was mathematically analysed by Madaki et al. [3]. Koriko et al. [4] discovered 3D Eyring–Powell nanofluid radiative flow temperature is lowered by the thermal stratification parameter. Besthapu et al. [5] found that as the temperature of the Casson nanofluid increases, so does the fluid's temperature. The radiation parameter reduces the Nusselt number, as discovered by Kotha et al. [6]. According to Dogonchi et al. [7], Rayleigh numbers have been shown to increase both Nusselt numbers (local and average). Shit and Mandal [8] and Raza [9] used an elongating surface to study distinct radiative Casson fluids (steady and unsteady). They concluded that the Biot number reduces entropy formation while the slip parameter increases surface drag force. Pordanjani et al. [10] found that the Bejan number is reduced by the radiation parameter. Radiative EMHD micropolar fluid flow via an elongating sheet was studied by Bilal [11] using an R–K integration approach. Different scientists [12–14] then examined various radiative nanofluid flows through varied geometrical configurations. They concluded that Lewis's number reduced fluid concentration, Brickman's improved entropy production, and Prandtl's reduced temperature. Thermal radiation has recently been studied, and diverse HNF (hybrid nanofluid) flows have been described through varied geometries [15–20].

Viscous dissipation has a substantial impact on incompressible fluid flows with high velocity. For the first time, Soundalgekar [21] used the name Eckert number to refer to the parameter of viscous dissipation. According to Jusoh et al. [22], the Eckert number reduces heat transmission. Non-Newtonian (pseudo-plastic) nanofluids demonstrate higher thermal performance than Newtonian (nano) fluids in the suction situation (Maleki et al. [23]). Dissipative micropolar flow at a stagnation point was explored by Kumar et al. [24] using an uneven elongating sheet. An increase in Eckert number, as seen by Afridi and Qasim [25] in the Blasius flow by a flat plate, increases fluid temperature. Dissipative nanofluid flows were afterwards researched by a number of writers [26–30]. Pressure gradient reduces velocity and the thermophoresis parameter raises temperature, to name a few of their results. A non-uniform elongating sheet was explored by Gayatri et al. [31] to explain Carreau fluid flow. Fluid concentration dropped with increasing chemical reaction, according to the researchers. In order to solve the problem of MHD fluid flow via an upright permeable plate, Chiranjeevi et al. [32] used the shooting approach. In their study of the dissipative flow of MHD fluid around an extended rotating disc, Abbas et al. [33] found that Bejan number and entropy production behave in the opposite direction of Brinkman number. Authors [34–39] have recently discussed several dissipative fluid flows in different geometries.

Researchers are currently focusing on the issue of heat transmission in industrial processes as their primary focus. Conventional cooling liquids such as ethylene glycol, water, and oil have been used in these procedures in the past, but their heat transfer rates are restricted. The usage of nanofluids in industrial processes has been introduced as an intriguing new type of heat transfer fluid. Shock absorbers and heat exchangers are just a couple of the many uses for nanofluid. The term “hybrid nanoparticles” refers to nanoparticles made up of two or more nanometer-sized components. Hybrid nanofluids are fluids created with hybrid nanoparticles. In addition to solar collectors and military equipment, they may be found in a number of areas including heat exchanger, automotive industry, transformer cooling and electronic cooling. According to Khan et al. [40], increasing the rotation parameter of hybrid nanofluid between parallel plates increases velocity. Three-dimensional MHD HNF (AA7072-AA7075/methanol) slip flow was studied by Tlili et al. [41]. They found that mono nanofluid surpasses hybrid nanofluid when it comes

to the Lorentz force. A number of studies have also been conducted on various hybrid nanofluids with different geometries [42–48].

Following a careful examination of the aforementioned literature, we discovered that when thermal radiation and viscous dissipation are significant, nothing is known about the dynamics of chemically reactive polyethylene glycol and water–zirconia–magnesium oxide hybrid nanofluid over a curved shrinking sheet at different levels of Lorentz force. Filling this void is the originality of this paper, i.e., examining the significance of chemical reaction on the radiative hybrid nanofluid flow by a curved shrinking sheet with viscous dissipation and magnetic field parameters. In this study, physical factors such as the skin friction coefficient (surface drag force) are statistically examined (through the correlation coefficient). Results were given on two separate occasions, i.e., binary (hybrid) nanofluid (polyethylene glycol and water–zirconia–magnesium oxide) and mono nanofluid (polyethylene glycol and water–zirconia). In addition, we checked our findings against those of other researchers and discovered a respectable degree of agreement.

## 2. Problem Formulation

We consider two-dimensional laminar, steady, and free convection flow of hybrid nanofluid through a curved shrinking sheet. Hybrid nanofluid is a combination of polyethylene glycol–water (base fluid), zirconia and magnesium oxide (nanoparticles). Assumptions for this flow are:

- Velocity of the sheet is denoted by  $u_w = cs$  where  $c < 0$  corresponds to shrinking;
- $R$  is the radius of the circular nest in which the curved sheet is enclosed;
- The strength of the magnetic field, denoted by the symbol  $B_0$ , is applied in the  $r$ – direction (see Figure 1), i.e., a magnetic field of uniform strength  $B_0$  is applied transversely to the direction of the flow;
- $C_\infty$  and  $C_w$  designate the ambient and surface concentrations while  $T_\infty$  and  $T_w$  designate the ambient and surface temperatures correspondingly;
- Higher order chemical reaction parameter is included in the diffusion equation to describe the mass transport phenomena. Thermal radiation and viscous dissipation parameters are included in the energy equation to describe the heat transport phenomena;
- Table 1 exhibits the values of thermo-physical properties of base fluid and nanomaterials involved in the hybrid nanofluid;
- Because it is so little in comparison to the external magnetic field, the induced magnetic field is ignored.

**Table 1.** Aspects of thermophysical relevant to HNF (Hossainy and Eid [47]).

S.No.		Polyethylene Glycol–Water Mixture ( $f$ )	ZrO <sub>2</sub> ( $s_1$ )	MgO ( $s_2$ )
1	$\rho$ (Kg/m <sup>3</sup> )	1110	5680	3560
2	$C_p$ (J/KgK)	3354	502	955
3	$k$ (W/mK)	0.3712	1.7	45
4	$\sigma$ (S/m)	-	$3 \times 10^{-5}$	-

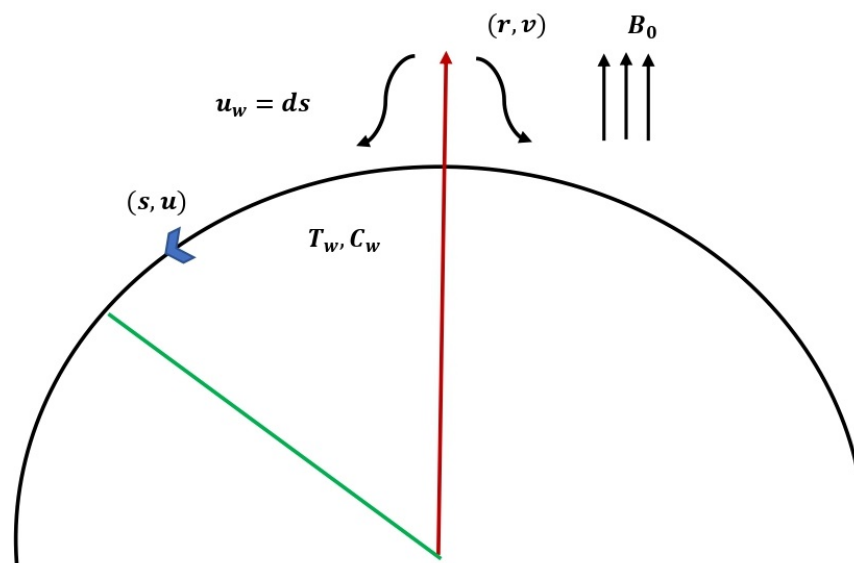


Figure 1. Flow design of the present study.

Taking into account the above assumptions, conservation of mass Equation (1), conservation of momentum Equations (2) and (3), conservation of energy Equation (4) and diffusion Equation (5) are presented below [46,47]:

$$\frac{\partial}{\partial r}[(R+r)v] + \frac{\partial u}{\partial s}R = 0 \tag{1}$$

$$u \frac{u}{R+r} = \frac{1}{\rho_{hnf}} \frac{\partial p}{\partial r} \tag{2}$$

$$\rho_{hnf} \left( \frac{\partial u}{\partial r} v + \frac{R}{R+r} \frac{\partial u}{\partial s} u + \frac{vu}{R+r} \right) = -\frac{R}{R+r} \frac{\partial P}{\partial s} + \left( \frac{\partial}{\partial r} \left( \frac{\partial u}{\partial r} \right) + \frac{\partial u}{\partial r} \frac{1}{R+r} - \frac{u}{R+r} \frac{1}{(R+r)} \right) \mu_{hnf} - u B_0^2 \sigma \tag{3}$$

$$(\rho C_p)_{hnf} \left( \frac{\partial T}{\partial r} v + \frac{\partial T}{\partial s} \frac{R}{R+r} u \right) = \left( \frac{\partial}{\partial r} \left( \frac{\partial T}{\partial r} \right) + \frac{\partial T}{\partial r} \frac{1}{R+r} \right) k_{hnf} + \left( \frac{\partial^2 T}{\partial r^2} + \frac{1}{R+r} \frac{\partial T}{\partial r} \right) \frac{16 T_{\infty}^3 \sigma^*}{3 k^*} + \left( \frac{\partial u}{\partial r} \right) \left( \frac{\partial u}{\partial r} \right) \mu_{hnf} \tag{4}$$

$$\frac{\partial C}{\partial r} v + \frac{\partial C}{\partial s} \frac{R}{R+r} u = \left( \frac{\partial}{\partial r} \left( \frac{\partial C}{\partial r} \right) + \frac{1}{R+r} \frac{\partial C}{\partial r} \right) D_m - \bar{R} (C - C_{\infty})^n \tag{5}$$

and the corresponding boundary conditions are:

$$\left. \begin{aligned} u(0, s) = u_w, v(0, s) = -v_w, T(0, s) = T_w, C(0, s) = C_w \\ u(r, s) \rightarrow 0, \frac{\partial u(r, s)}{\partial r} \rightarrow 0, T(r, s) \rightarrow T_{\infty}, C(r, s) \rightarrow C_{\infty} \text{ as } r \rightarrow \infty \end{aligned} \right\} \tag{6}$$

Thermo-physical properties of hybrid nanofluid are:

$$\left. \begin{aligned} (\rho C_p)_{hnf} &= (1 - \phi_2) \left[ (1 - \phi_1) (\rho C_p)_f + \phi_1 (\rho C_p)_{s_1} \right] + (\rho C_p)_{s_2} \phi_2, \\ \mu_{hnf} &= \frac{\mu_f}{(1 - \phi_1)^{2.5} (1 - \phi_2)^{2.5}}, \rho_{hnf} = (1 - \phi_2) \left[ (1 - \phi_1) \rho_f + \phi_1 \rho_{s_1} \right] + \rho_{s_2} \phi_2, \\ k_{hnf} &= \frac{k_{s_2} + 2k_{nf} - 2k_{nf} \phi_2 + 2k_{s_2} \phi_2}{k_{s_2} + 2k_{nf} + k_{nf} \phi_2 - k_{s_2} \phi_2} \times k_{nf}, k_{nf} = \frac{k_{s_1} + 2k_f - 2k_f \phi_1 + 2k_{s_1} \phi_1}{k_{s_1} + 2k_f + k_f \phi_1 - k_{s_1} \phi_1} \times k_f \end{aligned} \right\}$$

Similarity transformations (Abbas et al. [46])

$$\left. \begin{aligned} \eta = \sqrt{\frac{dr^2}{v_f}}, p = \rho_f d^2 s^2 P(\eta), u = ds f'(\eta), v = -\frac{1}{R+r} \sqrt{dv_f} R f(\eta), \\ T = T_{\infty} - (T_{\infty} - T_w) \theta(\eta), C = C_{\infty} - (C_{\infty} - C_w) \Phi(\eta) \end{aligned} \right\} \tag{7}$$

satisfy the continuity Equation (1) and transform Equations (2)–(5) as follows:

$$P' = \frac{f'}{K + \eta} f' \tag{8}$$

$$\frac{2}{L_1} \frac{K}{K + \eta} P = \left( f''' + f'' \frac{1}{K + \eta} - \frac{1}{K + \eta} \frac{f'}{(\eta + K)} \right) \frac{1}{L_1 L_2} + \left( f f'' - f'^2 + \frac{1}{K + \eta} f f' \right) \frac{K}{K + \eta} - \frac{M}{L_1} f' \tag{9}$$

$$\theta'' + \frac{1}{K + \eta} \theta' + \frac{L_4}{Ra + L_3 L_{31}} \left( \text{Pr} f \frac{K}{K + \eta} \theta' + \text{Pr} f'' \frac{1}{L_2 L_4} E_{ck} f'' \right) = 0 \tag{10}$$

$$\Phi'' + \frac{1}{K + \eta} \Phi' + \left( f \frac{K}{K + \eta} \Phi' - Kr \Phi'' \right) Sc = 0 \tag{11}$$

and transform the boundary conditions in (6) as:

$$\left. \begin{aligned} f(\eta) = S, f'(\eta) = \delta, \theta(\eta) = 1, \Phi(\eta) = 1 \text{ at } \eta = 0 \\ f'(\eta) \rightarrow 0, f''(\eta) \rightarrow 0, \theta(\eta) \rightarrow 0, \Phi(\eta) \rightarrow 0 \text{ as } \eta \rightarrow \infty \end{aligned} \right\} \tag{12}$$

Here:

$$\left. \begin{aligned} L_1 = \left[ (1 - \phi_1) + \phi_1 \frac{\rho_{s1}}{\rho_f} \right] (1 - \phi_2) + \frac{\rho_{s2}}{\rho_f} \phi_2, L_2 = (1 - \phi_2)^{2.5} (1 - \phi_1)^{2.5}, L_{31} = \frac{k_{s1} + 2k_f + 2\phi_1(-k_f + k_{s1})}{k_{s1} + 2k_f - \phi_1(-k_f + k_{s1})}, \\ L_3 = \frac{k_{s2} + 2L_{41}k_f + 2\phi_2(-L_{41}k_f + k_{s2})}{k_{s2} + 2L_{41}k_f - \phi_2(-L_{41}k_f + k_{s2})}, L_4 = \left[ (1 - \phi_1) + \phi_1 \frac{(\rho C_p)_{s1}}{(\rho C_p)_f} \right] (1 - \phi_2) + \frac{(\rho C_p)_{s2}}{(\rho C_p)_f} \phi_2 \end{aligned} \right\}$$

and:

$$\left. \begin{aligned} K = R \sqrt{\frac{d}{v_f}}, E_{ck} = \frac{d^2 s^2}{(C_p)_f (T_w - T_\infty)}, M = \frac{\sigma B_0^2}{\rho_f d}, Ra = \frac{16 T_\infty^3 \sigma^*}{3 k^* k}, \text{Pr} = \frac{\mu_f (C_p)_f}{k_f}, \\ Kr = \frac{\bar{R} (C_w - C_\infty)^{n-1}}{d}, Sc = \frac{v_f}{D_m}, \delta = \frac{c}{d} \end{aligned} \right\}$$

From Equation (9), we can obtain:

$$P = \frac{L_1}{2} \frac{K + \eta}{K} \left[ \frac{1}{2L_2} \left( f''' + \frac{1}{K + \eta} f'' - \frac{f'}{(\eta + K)^2} \right) + \frac{K}{K + \eta} \left( f f'' - f'^2 + f \frac{1}{K + \eta} f' \right) - M \frac{L_3 L_{31}}{L_1} f' \right]. \tag{13}$$

From Equations (8) and (13), we can obtain the momentum equation as:

$$\begin{aligned} f^{iv} + \frac{1}{K + \eta} \frac{f'}{(K + \eta)^2} + \left[ \frac{K}{K + \eta} (f''' f - f'' f') + \frac{K}{(K + \eta)} (f'' f + f'^2) \frac{1}{K + \eta} - \frac{K}{(K + \eta)^2} \frac{1}{K + \eta} f f' \right] L_1 L_2 \\ - L_2 \left( M f'' + M \frac{1}{K + \eta} f' \right) - 2L_1 L_2 \frac{1}{K + \eta} \frac{K}{(K + \eta)} f'^2 + \frac{2}{K + \eta} f''' - \frac{1}{(K + \eta)^2} f'' = 0 \end{aligned} \tag{14}$$

Nusselt number  $Nu_s$ , Friction factor  $C_{fs}$ , Sherwood number  $Sh_s$  are indicated as:

$$Nu_s = \frac{sq_w}{(T_w - T_\infty)k_f}, C_{fs} = \frac{2\tau_{rs}}{\rho_f u_w^2}, Sh_s = \frac{sj_w}{(C_w - C_\infty)D_m} \tag{15}$$

where  $q_w = -\left(\frac{\partial T}{\partial r}\right)k_{hnf}\Big|_{r=0}$  (heat flux),  $\tau_{rs} = \mu_{hnf}\left(\frac{\partial u}{\partial r} - \frac{u}{r+R}\right)\Big|_{r=0}$  (wall shear stress),

$$j_w = -\left(\frac{\partial C}{\partial r}\right)D_m\Big|_{r=0} \text{ (mass flux)}. \tag{16}$$

With the assistance of (7), terms in (15) can be redrafted as:

$$\left. \begin{aligned} (\text{Re}_s)^{0.5} C_{fs} = \frac{1}{L_2} \left( f''(0) - \frac{1}{K} f'(0) \right), \\ (\text{Re}_s)^{-0.5} Nu_s = -\frac{k_{hnf}}{k_{nf}} \theta'(0), (\text{Re}_s)^{-0.5} Sh_s = -\Phi'(0) \end{aligned} \right\} \tag{17}$$

where  $Re_s = \frac{su_w}{\nu_f}$  (Reynold’s number).

### 3. Numerical Procedure

Bvp4c is a built-in function in MATLAB that solves Equations (10), (11) and (14) using boundary conditions (12). The bvp4c solver is a built-in function, making it easy to use.

As a pre-process to write the code, we first need to adopt the following assumptions (Waini et al. [48]):

$$x_1 = f, x_2 = f', x_3 = f'', x_4 = f''', x_5 = \theta, x_6 = \theta', x_7 = \Phi, x_8 = \Phi'$$

Then, using the Equations (10), (11) and (14) with conditions (12), we can develop a subsequent system of ODEs of first order:

$$\left. \begin{aligned} x_1' &= x_2, \\ x_2' &= x_3, \\ x_3' &= x_4, \\ x_4' &= - \left( \frac{2}{K+\eta} x_4 + \left[ \frac{K}{K+\eta} (x_1 x_4 - x_2 x_3) + \frac{K}{(K+\eta)} (x_1 x_3 + x_2^2) \frac{1}{K+\eta} - \frac{K}{(K+\eta)^2} \frac{1}{K+\eta} x_1 x_2 \right] L_1 L_2 \right) \\ &\quad - L_2 \left( M x_3 + M \frac{1}{K+\eta} x_2 \right) - 2 L_1 L_2 \frac{1}{K+\eta} \frac{K}{(K+\eta)} x_2^2 + \frac{1}{K+\eta} \frac{x_2}{(K+\eta)^2} - \frac{1}{(K+\eta)^2} x_3 \\ x_5' &= x_6, \\ x_6' &= - \left( \frac{1}{K+\eta} x_6 + \frac{L_4}{Ra+L_3 L_{31}} \left( Pr x_1 \frac{K}{K+\eta} x_6 + Pr \frac{1}{L_2 L_4} E_{ck} x_3^2 \right) \right), \\ x_6' &= x_7, \\ x_7' &= - \left( \frac{1}{K+\eta} x_7 + Sc \left( \frac{K}{K+\eta} x_1 x_7 - Kr x_6^n \right) \right) \end{aligned} \right\}$$

with the conditions:

$$\left. \begin{aligned} xa(1) &= S, xa(2) = \delta, xa(5) = 1, xa(7) = 1 \\ xb(2) &= 0, xb(3) = 0, xb(5) = 0, xb(7) = 0 \end{aligned} \right\}$$

After converting the above system as a MATLAB code, we can execute it to obtain the required outcomes in the form of graphs.

### 4. Validation

The results of this study, in addition to prior studies, were subjected to rigorous testing, and the results were judged to be adequate (see Table 2).

**Table 2.** Local Nusselt number validation in restricted situations (for example,  $K \rightarrow \infty$  and  $\phi_1 = \phi_2 = 0$ ).

Pr	Mukhopadhyay [49]	Present Study
0.01	0.02944	0.029440
0.72	1.08855	1.088550
1.00	1.33334	1.333340
3.00	2.50972	2.509720

### 5. Discussion of the Outcomes

In this study, results for two scenarios, PEG – Water + ZrO<sub>2</sub> + MgO (hybrid nanofluid) and PEG – Water + ZrO<sub>2</sub>, (nanofluid) are reported. The streamlines for the current flow issue are shown in Figure 2.

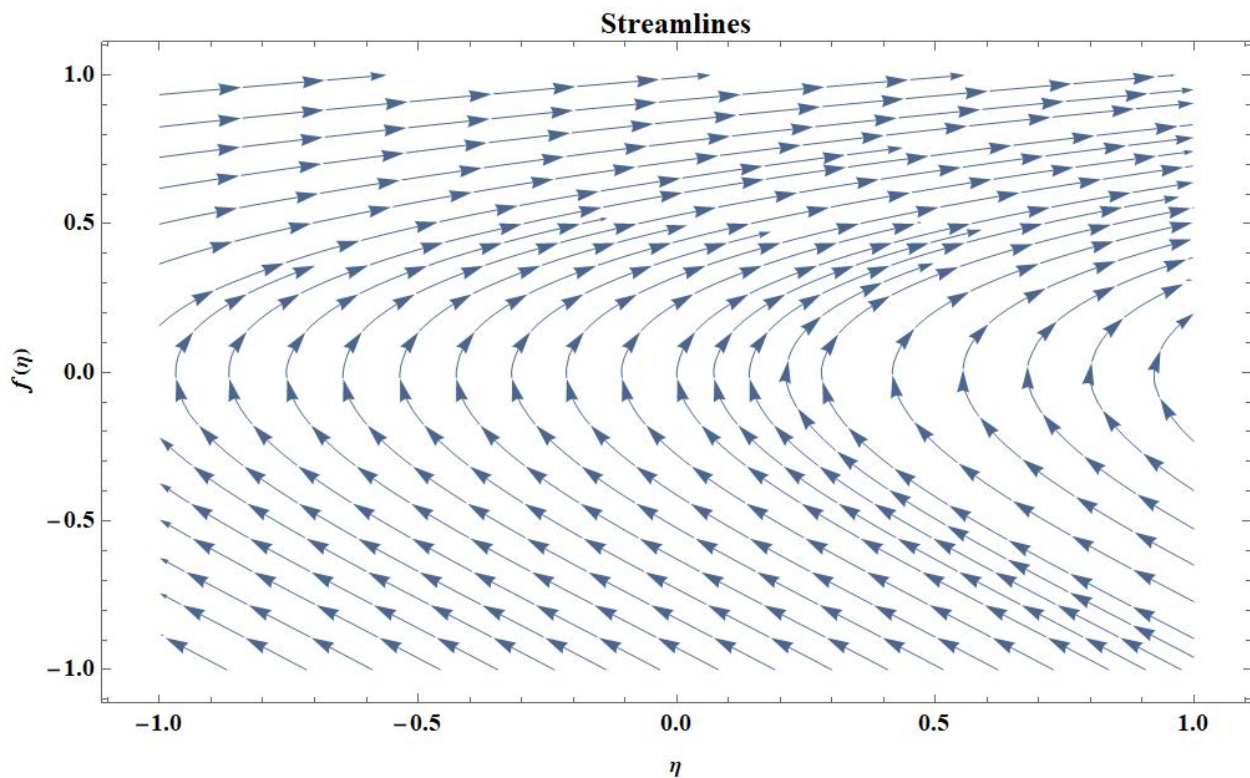


**Figure 2.** Streamlines of the present flow.

### 5.1. Engineering Parameters of Interest

It is clear from Figures 3 and 4 that the volume fraction of nanoparticles enhances the skin friction coefficient and curvature parameter lessens the same. It was noticed that, when radius of curvature parameter ( $K$ ) takes input in the range  $0.5 \leq K \leq 2.5$ , the skin friction coefficient decreases at a rate of 1.46633 (i.e., 146.633%) (in the case of hybrid nanofluid) and 1.11236 (i.e., 111.236%) (in the case of nanofluid) per unit value of radius of curvature parameter. Increasing rates in the skin friction parameter are 3.481179 (i.e., 348.1179%) (in the case of hybrid nanofluid) and 2.745679 (i.e., 274.5679%) (in the case of nanofluid) when the volume fraction of nanoparticle ( $\phi_1$ ) takes input in the range  $0 \leq \phi_1 \leq 0.2$ . Nusselt number drops as Eckert number and curvature parameter rise, as shown in Figures 5 and 6. The decrement rates were observed as 1.41148 (i.e., 141.148%) (in the case of hybrid nanofluid) and 1.15337 (i.e., 115.337%) (in the case of nanofluid) when Eckert number takes input in the range  $0 \leq E_{ck} \leq 0.2$ . In addition, it was revealed that increasing  $Kr$  and  $Sc$  speeds up mass transfer rate (Figures 7 and 8). When chemical reaction parameter takes input in the range  $0 \leq Kr \leq 0.4$ , increment rates in mass transfer rate are 1.497214 (i.e., 149.7214%) (in the case of hybrid nanofluid) and 1.496621 (i.e., 149.6621%) (in the case of nanofluid) whereas increment rates in the same against  $Sc$  are 1.711774 (i.e., 171.2774%) (in the case of hybrid nanofluid) and 1.710781 (i.e., 171.0781%) (in the case of nanofluid) with the range  $0 \leq Sc \leq 0.4$ .

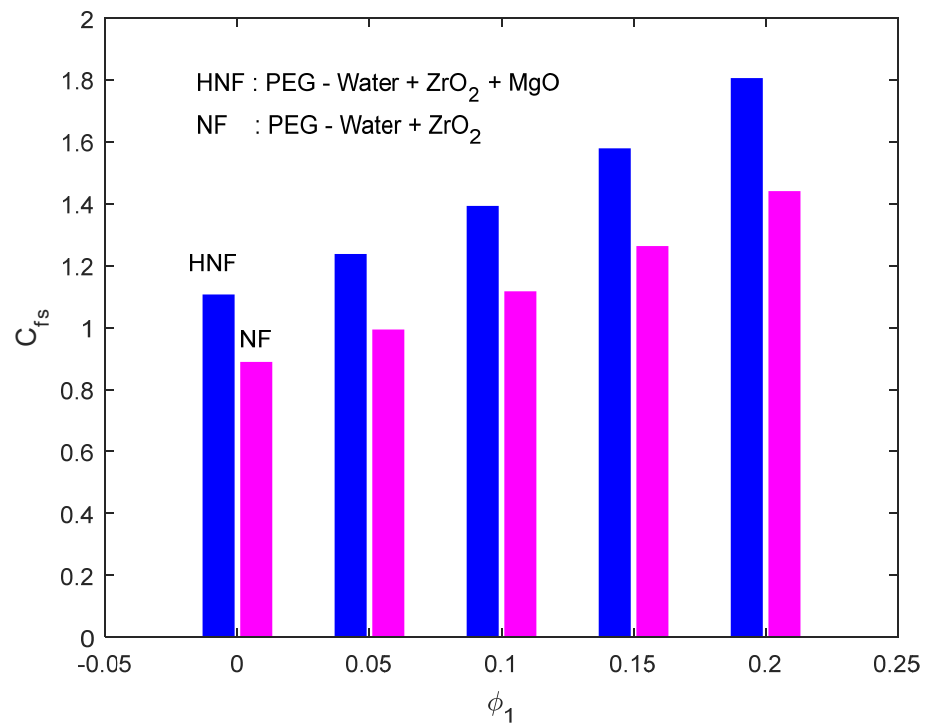


Figure 3. Effects on skin friction coefficient due to  $\phi_1$ .

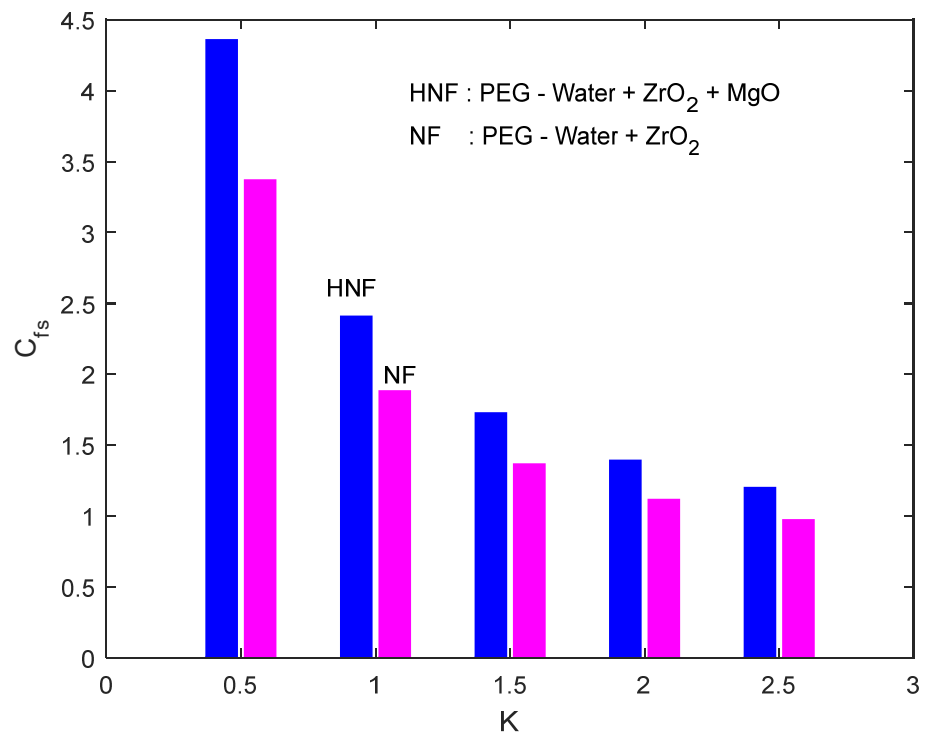


Figure 4. Effects on skin friction coefficient due to K.



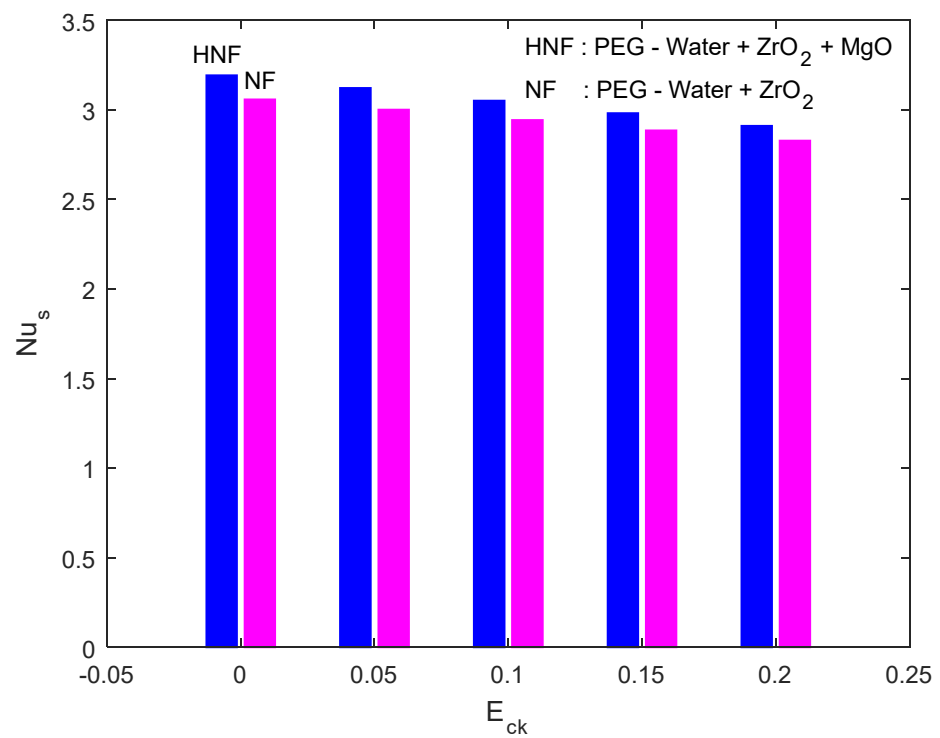


Figure 5. Effects on heat transfer rate due to  $E_{ck}$ .

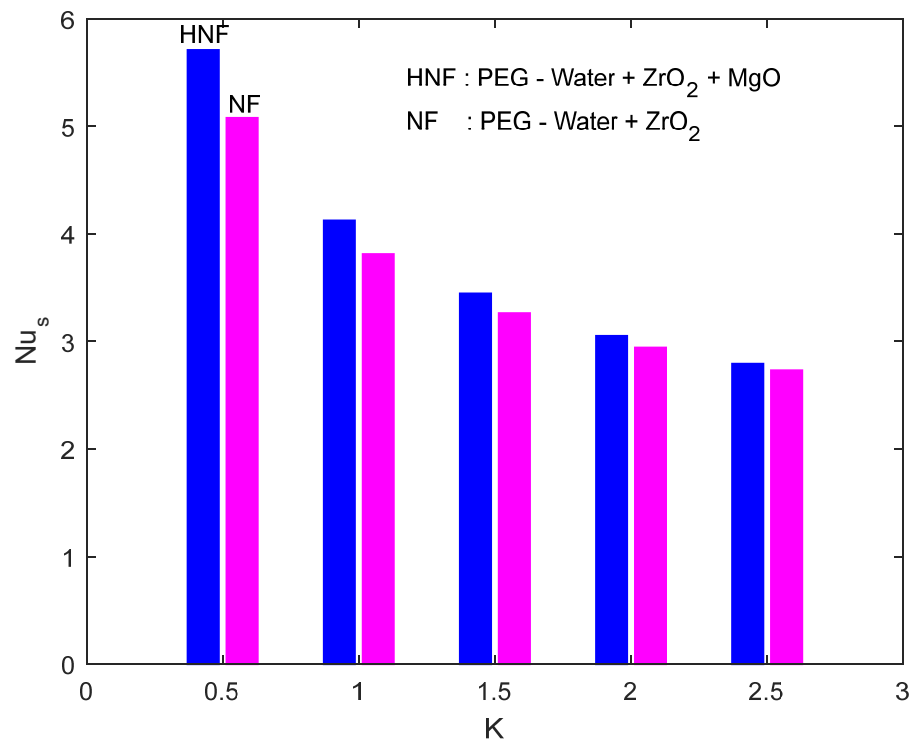


Figure 6. Effects on heat transfer rate due to  $K$ .

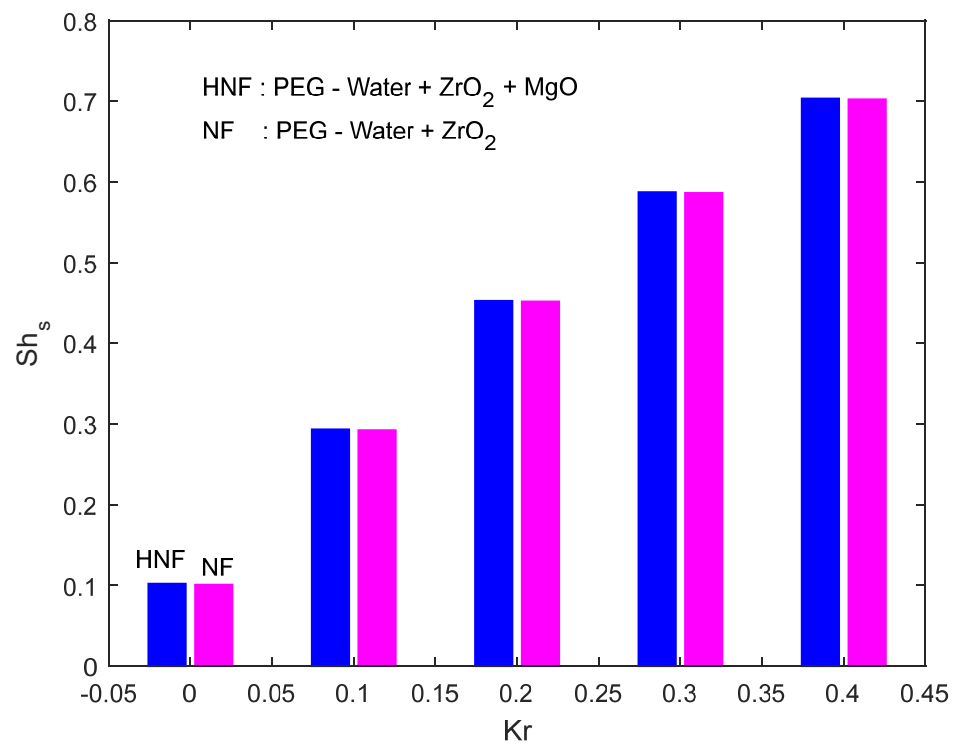


Figure 7. Effects on mass transfer rate due to  $Kr$ .

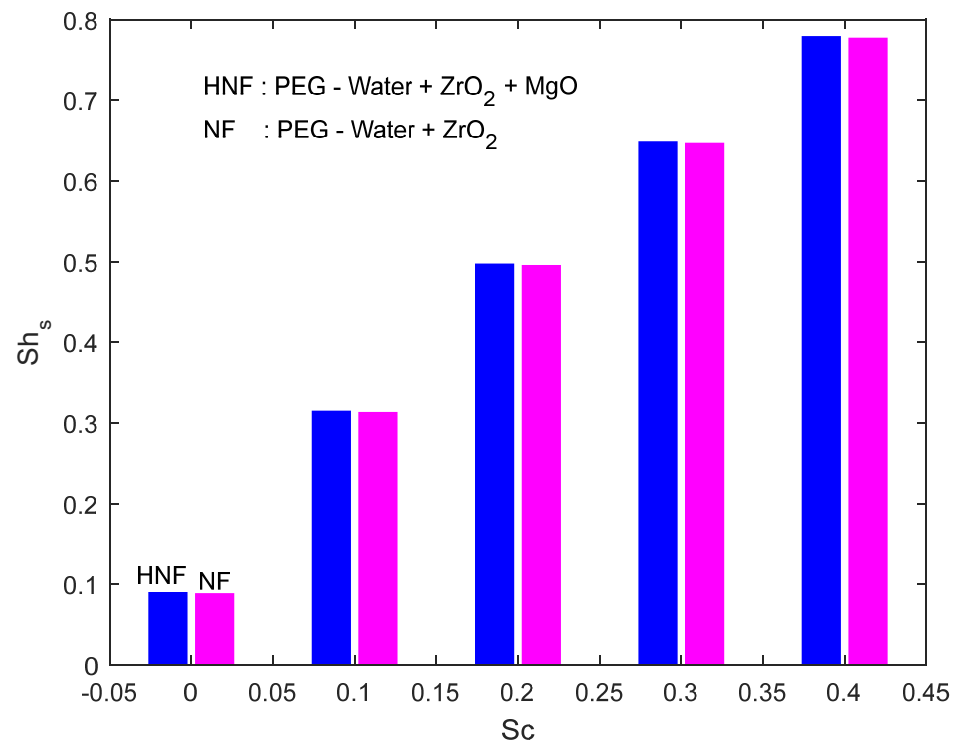


Figure 8. Effects on mass transfer rate due to  $Sc$ .

### 5.2. Statistical Analysis of Physical Parameters Using Correlation Coefficient

Shear stress and other physical properties were substantiated by a statistical analysis using a correlation coefficient.

Coefficient of correlation is a numerical indicator of the link between two variables.  $-1$  (negative correlation) to  $1$  (positive correlation) are the possible values for the coefficient.

The correlation coefficient ( $\lambda$ ) can be calculated using:

$$\lambda = \frac{q(\sum yz) - (\sum y)(z)}{\sqrt{[q\sum y^2 - (\sum y)^2][q\sum z^2 - (\sum z)^2]}}$$

In order to determine the correctness and dependability of the coefficient value, the *P.E.* (probable error) of the correlation coefficient is helpful. The significance of the correlation is determined by the relationship between the coefficient value ( $\lambda$ ) and *P.E.* If  $\frac{|\lambda|}{P.E} > 6$  (or  $|\lambda| > 6P.E$ ), we say the correlation is substantial; otherwise, we say the connection is insignificant.

One can evaluate *P.E.* by using  $P.E = 0.6745 \frac{1-\lambda^2}{\sqrt{q}}$  where  $q$  is the number of observations.

Table 3 shows that the skin friction coefficient is positively correlated with  $\phi_1$  and negatively correlated with  $K$ . That is, the skin friction coefficient declines as  $K$  increases and increases as  $\phi_1$  increases. The link between the parameters ( $E_{ck}$ ,  $K$ ) and heat transfer rate was detailed in Table 4. It was observed that all those parameters have a strong negative association with the Nusselt number (may be due to the escalation in thermal boundary layer thickness). Table 5 shows that there is a considerable positive relationship between  $Sc$ ,  $Kr$  and mass transfer rate.

**Table 3.** Shear stress and a few other factors' connection.

	$C_{fx}$					
	PEG–Water+ZrO <sub>2</sub> +MgO			PEG–Water+ZrO <sub>2</sub>		
	$\lambda$	<i>P.E.</i>	$\frac{ \lambda }{P.E}$	$\lambda$	<i>P.E.</i>	$\frac{ \lambda }{P.E}$
$\phi_1$	0.9941	0.003548	280.18	0.9946	0.004816	206.52
$K$	−0.9042	0.055026	16.43	−0.9027	0.055844	16.16

**Table 4.** Some factors' link with heat transfer rate.

	$Nu_x$					
	PEG–Water+ZrO <sub>2</sub> +MgO			PEG–Water+ZrO <sub>2</sub>		
	$\lambda$	<i>P.E.</i>	$\frac{ \lambda }{P.E}$	$\lambda$	<i>P.E.</i>	$\frac{ \lambda }{P.E}$
$E_{ck}$	−0.9999	0.000029	34479.31	−0.9999	0.000029	34,479.31
$K$	−0.9580	0.012104	79.15	−0.9587	0.011907	80.52

**Table 5.** Some factors' link with mass transfer rate.

	$Sh_x$					
	PEG–Water+ZrO <sub>2</sub> +MgO			PEG–Water+ZrO <sub>2</sub>		
	$\lambda$	<i>P.E.</i>	$\frac{ \lambda }{P.E}$	$\lambda$	<i>P.E.</i>	$\frac{ \lambda }{P.E}$
$Sc$	0.9994	0.000177	5646.33	0.9994	0.000177	5646.33
$Kr$	0.9998	0.000059	16,945.76	0.9998	0.000059	16,945.76

### 5.3. Regular Profiles including Velocity Profile

The fluid's viscosity increases as the volume fraction of nanoparticles increases, obstructing fluid flow. Because of this, the velocity decreases with increasing size of  $\phi_1$  (Figure 9). Figure 10 shows that the radius of curvature parameter has a negative effect on velocity profile (curvature parameter is proportional to the surface radius of the shrinking sheet). More nanoparticle interaction is often observed when the volume percentage of the particles increases. As a result, the temperature rises as the fluid grows hotter (Figure 11). Figure 12 shows that as the value of  $E_{ck}$  increases, so does the fluid temperature. Because of frictional

heating, heat is produced in the fluid as the value of  $E_{ck}$  increases. Eckert number is the physical ratio of kinetic energy to the specific enthalpy difference between the wall and the fluid. As a result, increasing the Eckert number causes the transformation of kinetic energy into internal energy via work conducted against viscous fluid stresses. As a result, increasing  $E_{ck}$  raises the temperature of the fluid. When thermal radiation is delivered to a fluid, the fluid absorbs it, resulting in an increase in the fluid's heat energy. As a result, the fluid's temperature improves (Figure 13). Concentration typically decreases as the chemical reaction parameter increases (Figure 14). Entropy formation might be a possible explanation for this behaviour. When  $Sc$  increases, momentum diffusivity far exceeds mass diffusivity, implying that the fluid moves at a high velocity and fluid concentration decreases (Figure 15).

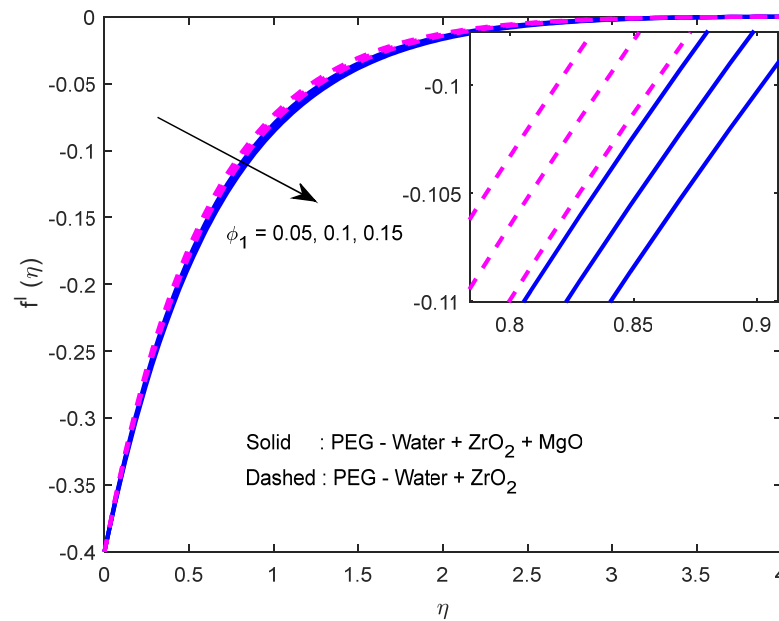


Figure 9. Effects on velocity due to  $\phi_1$ .

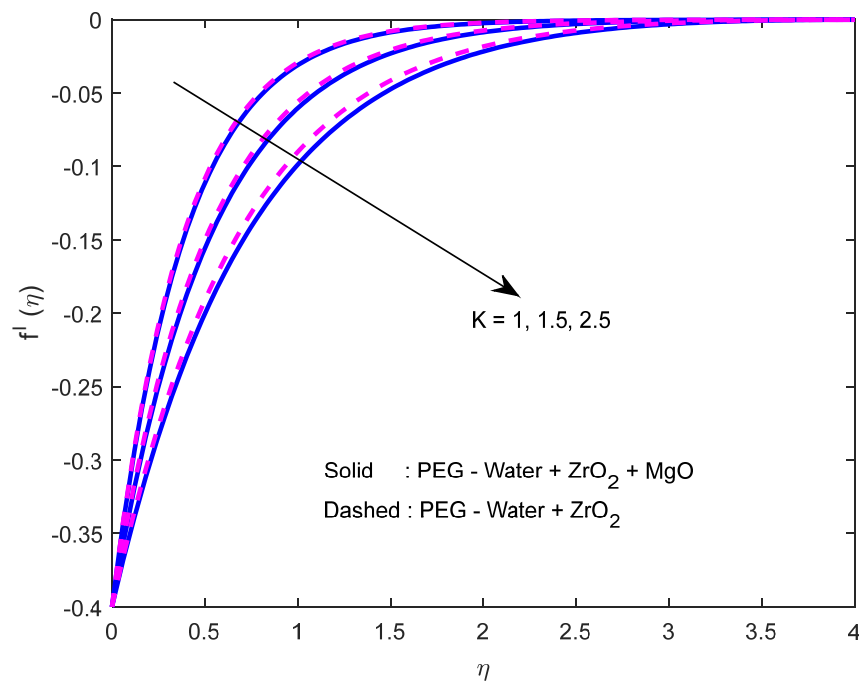


Figure 10. Effects on velocity due to  $K$ .

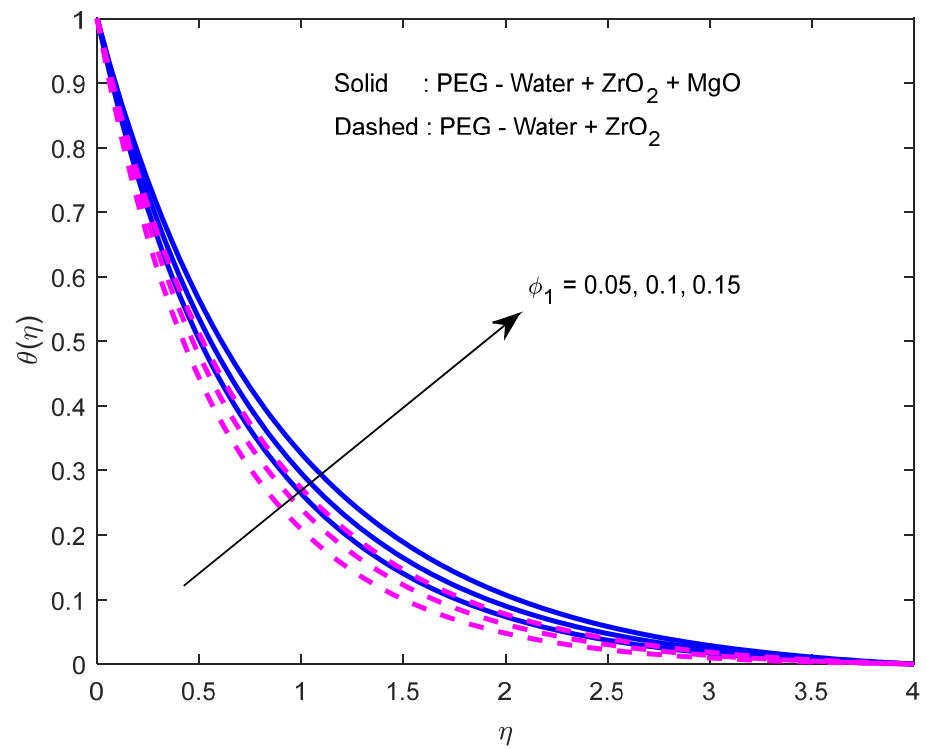


Figure 11. Effects on velocity due to  $\phi_1$ .

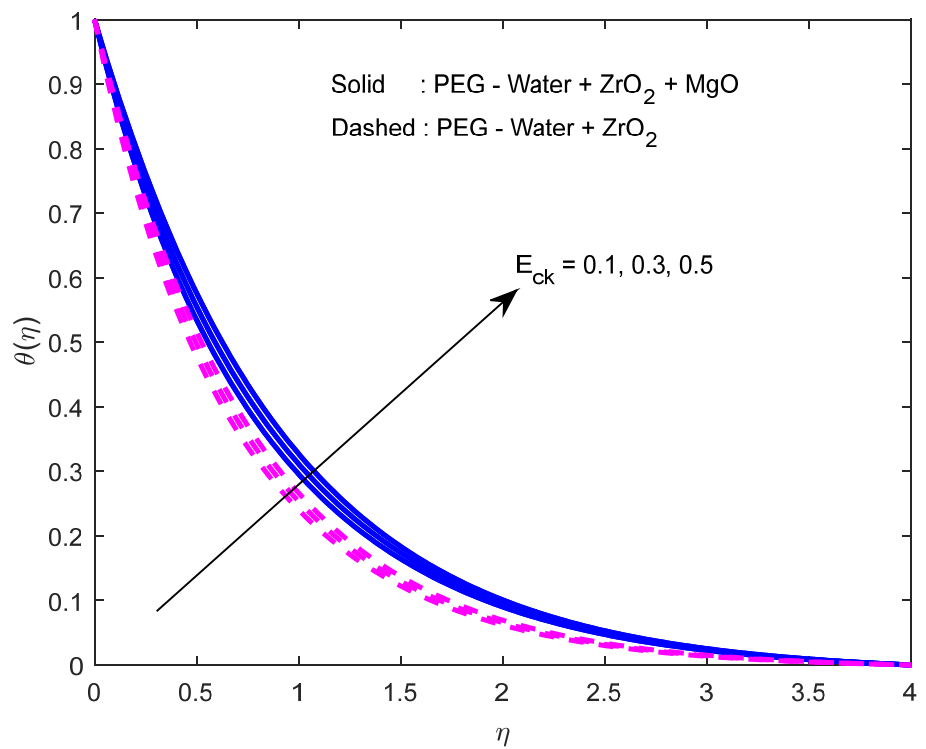


Figure 12. Effects on temperature due to  $E_{ck}$ .

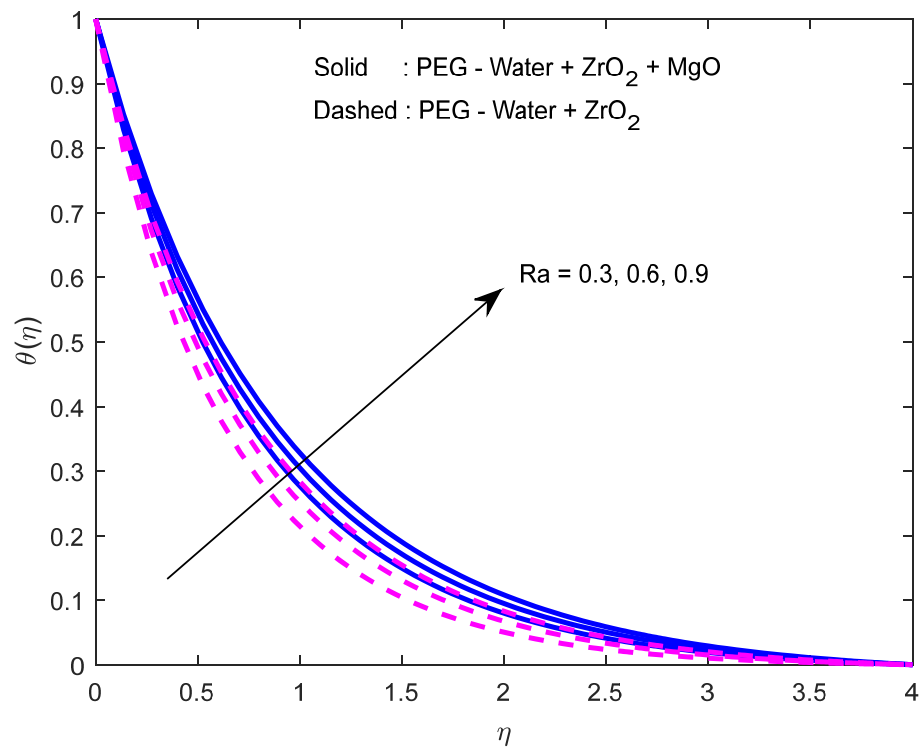


Figure 13. Effects on temperature due to  $Ra$ .

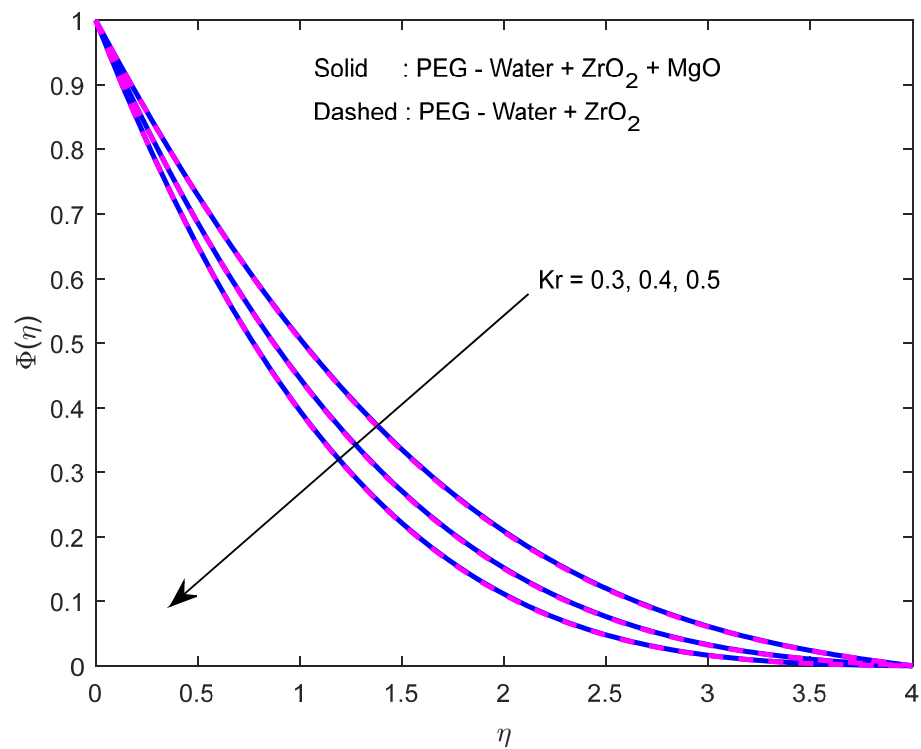


Figure 14. Effects on concentration due to  $Kr$ .

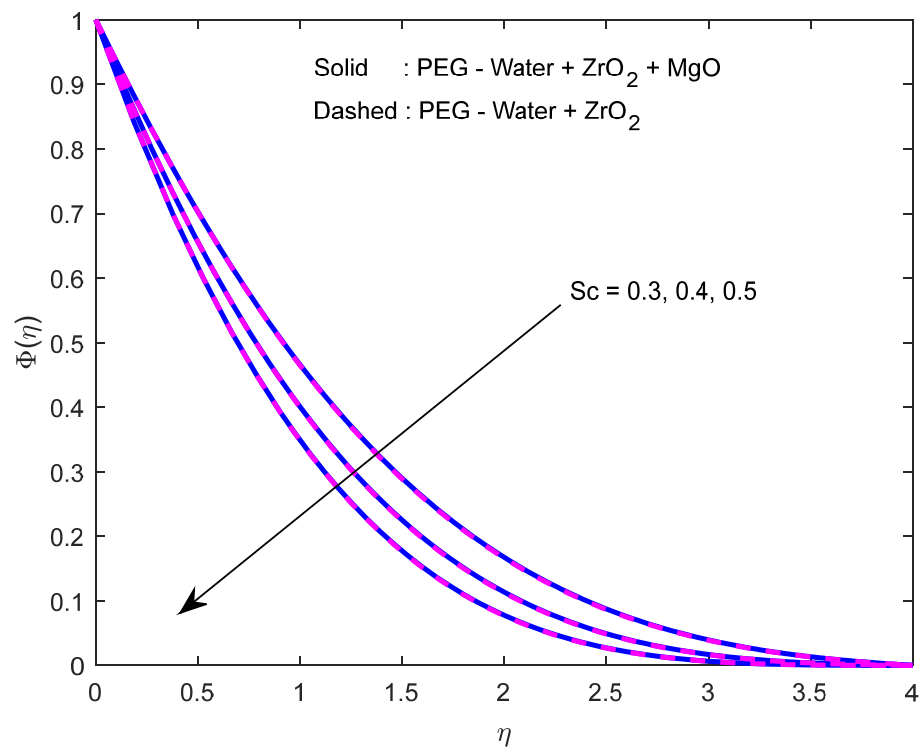


Figure 15. Effects on concentration due to  $Sc$ .

### 6. Conclusions

When thermal radiation and chemical reaction are significant, a comparative analysis between the dynamics of polyethylene glycol–water–zirconium oxide nanofluid and polyethylene glycol–water–zirconium dioxide–magnesium oxide hybrid nanofluid over a curved shrinking sheet at different levels of Lorentz force and viscous dissipation, has been explored. Based on the analysis and discussion of the results, it is worthy to conclude that:

- It was noticed that, when radius of curvature parameter ( $K$ ) takes input in the range  $0.5 \leq K \leq 2.5$ , the skin friction coefficient decreases at a rate of 1.46633 (i.e., 146.633%) (in the case of hybrid nanofluid) and 1.11236 (i.e., 111.236%) (in the case of nanofluid) per unit value of curvature parameter;
- It was detected that, when Eckert number ( $E_{ck}$ ) increases, Nusselt number decreases. The decrement rates were observed as 1.41148 (i.e., 141.148%) (in the case of hybrid nanofluid) and 1.15337 (i.e., 115.337%) (in the case of nanofluid) when Eckert number takes input in the range  $0 \leq E_{ck} \leq 0.2$ ;
- It was revealed that increasing  $Kr$  and  $Sc$  speeds up mass transfer rate. When chemical reaction parameter takes input in the range  $0 \leq Kr \leq 0.4$ , increment rates in mass transfer rate were 1.497214 (i.e., 149.7214%) (in the case of hybrid nanofluid) and 1.496621 (i.e., 149.6621%) (in the case of nanofluid) whereas increment rates in the same against  $Sc$  were 1.711774 (i.e., 171.1774%) (in the case of hybrid nanofluid) and 1.710781 (i.e., 171.0781%) (in the case of nanofluid) with the range  $0 \leq Sc \leq 0.4$ ;
- Fluid temperature rises as thermal radiation rises.

**Author Contributions:** Conceptualization, G.V. and N.A.S.; methodology, P.P. and H.K. software, M.J.B.; validation, M.J.B. and S.-J.Y.; formal analysis, C.S.K.R.; investigation, P.P.; resources, H.K. and S.H.; data curation, S.H.; Writing—original draft preparation, G.V., C.S.K.R. and N.A.S.; writing—review and editing, all authors; visualization, H.K.; supervision, S.-J.Y.; project administration, N.A.S., funding acquisition, S.-J.Y.; G.V. and N.A.S. collaborated equally to this work and are co-first authors. All authors have read and agreed to the published version of the manuscript.

**Funding:** This research received no external funding.

**Institutional Review Board Statement:** Not applicable.

**Informed Consent Statement:** Not applicable.

**Data Availability Statement:** The numerical data used to support the findings of this study are included within the article.

**Acknowledgments:** This research was conducted under the “Reduction Management Program of Fine Dust Blind-Spots” and was supported by the Ministry of Environment as part of the “Korea Environmental Industry & Technology Institute (KEITI) (No. 2020003060010)”.

**Conflicts of Interest:** The authors declare no conflict of interest.

## Nomenclature

$u, v$	Velocity components in $s, r$ directions [ $\text{ms}^{-1}$ ]
$p$	Dimensional fluid pressure [ $\text{Kgm}^{-1}\text{s}^{-2}$ ]
$P$	Dimensionless fluid pressure
$\mu$	Dynamic viscosity [ $\text{m}^2\text{s}^{-1}$ ]
$\rho$	Density [ $\text{Kgm}^{-3}$ ]
$\sigma$	Electrical conductivity [ $\text{Sm}^{-1}$ ]
$T$	Fluid temperature [K]
$k$	Thermal conductivity [ $\text{Wm}^{-1}\text{K}^{-1}$ ]
$\sigma^*$	Stefan–Boltzmann constant
$C_p$	Specific heat capacity [ $\text{JKgK}^{-1}$ ]
$k^*$	Mean absorption coefficient
$D_m$	Molecular diffusivity [ $\text{m}^2\text{s}^{-1}$ ]
$K$	Dimensionless radius of curvature
$\bar{R}$	Rate of chemical reaction
$v_w$	Permeability of the porous surface
$f'$	Fluid velocity
$Ra$	Radiation parameter
$\theta$	Fluid temperature
$\Phi$	Fluid concentration
$Pr$	Prandtl number
$M$	Magnetic field constraint
$E_{ck}$	Eckert number
$S$	Dimensionless suction/injection parameter
$n$	Order of chemical reaction
$C$	Dimensional concentration
$\delta$	Shrinking parameter
$Kr$	Chemical reaction parameter
$Sc$	Schmidt number
$\eta$	Similarity variable
Subscripts	
$f$	Fluid
$nf$	Mono nanofluid
$hnf$	Hybrid nanofluid
$s_1, s_2$	Nanomaterials (I, II)

## References

1. Ibrahim, F.S.; Hady, F.M. Mixed convection-radiation interaction in boundary-layer flow over horizontal surfaces. *Astrophys. Space Sci.* **1990**, *168*, 263–276. [[CrossRef](#)]
2. Bhatti, M.M.; Mishra, S.R.; Abbas, T.; Rashidi, M.M. A mathematical model of MHD nanofluid flow having gyrotactic microorganisms with thermal radiation and chemical reaction effects. *Neural Comput. Appl.* **2018**, *30*, 1237–1249. [[CrossRef](#)]
3. Madaki, A.; Roslan, R.; Rusiman, M.; Raju, C.S.K. Analytical and numerical solutions of squeezing unsteady Cu and TiO<sub>2</sub>-nanofluid flow in the presence of thermal radiation and heat generation/absorption. *Alex. Eng. J.* **2018**, *57*, 1033–1040. [[CrossRef](#)]



4. Koriko, O.K.; Animasaun, I.L.; Reddy, M.G.; Sandeep, N. Scrutinization of thermal stratification, nonlinear thermal radiation and quartic autocatalytic chemical reaction effects on the flow of three-dimensional Eyring-Powell alumina-water nanofluid. *Multidiscip. Model. Mater. Struct.* **2018**, *14*, 261–283. [[CrossRef](#)]
5. Besthapu, P.; Haq, R.U.; Bandari, S.; Al-Mdallal, Q.M. Thermal radiation and slip effects on MHD stagnation point flow of non-Newtonian nanofluid over a convective stretching surface. *Neural Comput. Appl.* **2017**, *31*, 207–217. [[CrossRef](#)]
6. Kotha, G.; Kukkamalla, K.; Ibrahim, S. Effect of thermal radiation on engine oil nanofluid flow over a permeable wedge under convective heating. *Multidiscip. Model. Mater. Struct.* **2019**, *15*, 187–205. [[CrossRef](#)]
7. Dogonchi, A.S.; Waqas, M.; Seyyedi, S.M.; Hashemi-Tilehnoee, M.; Ganji, D.D. Numerical simulation for thermal radiation and porous medium characteristics in flow of CuO-H<sub>2</sub>O nanofluid. *J. Braz. Soc. Mech. Sci. Eng.* **2019**, *41*, 1–13. [[CrossRef](#)]
8. Shit, G.C.; Mandal, S. Entropy Analysis on unsteady MHD flow of casson nanofluid over a stretching vertical plate with thermal radiation effect. *Int. J. Appl. Comput. Math.* **2019**, *6*, 2. [[CrossRef](#)]
9. Raza, J. Thermal radiation and slip effects on magnetohydrodynamic (MHD) stagnation point flow of Casson fluid over a convective stretching sheet. *Propuls. Power Res.* **2019**, *8*, 138–146. [[CrossRef](#)]
10. Pordanjani, A.H.; Aghakhani, S.; Karimipour, A.; Afrand, M.; Goodarzi, M. Investigation of free convection heat transfer and entropy generation of nanofluid flow inside a cavity affected by magnetic field and thermal radiation. *J. Therm. Anal.* **2019**, *137*, 997–1019. [[CrossRef](#)]
11. Bilal, M. Micropolar flow of EMHD nanofluid with nonlinear thermal radiation and slip effects. *Alex. Eng. J.* **2020**, *59*, 965–976. [[CrossRef](#)]
12. Kumar, B.; Srinivas, S. Unsteady hydromagnetic flow of Eyring-Powell Nanofluid over an inclined permeable stretching sheet with joule heating and thermal radiation. *J. Appl. Comput. Mech.* **2020**, *6*, 259–270.
13. Aziz, A.; Shams, M. Entropy generation in MHD Maxwell nanofluid flow with variable thermal conductivity, thermal radiation, slip conditions, and heat source. *AIP Adv.* **2020**, *10*, 015038. [[CrossRef](#)]
14. Reddy, P.S.; Sreedevi, P. Impact of chemical reaction and double stratification on heat and mass transfer characteristics of nanofluid flow over porous stretching sheet with thermal radiation. *Int. J. Ambient Energy* **2020**, *43*, 1626–1636. [[CrossRef](#)]
15. Hosseinzadeh, K.; Roghani, S.; Mogharrebi, A.R.; Asadi, A.; Ganji, D.D. Optimization of hybrid nanoparticles with mixture fluid flow in an octagonal porous medium by effect of radiation and magnetic field. *J. Therm. Anal.* **2020**, *143*, 1413–1424. [[CrossRef](#)]
16. Raju, S.S.K.; Babu, M.J.; Raju, C.S.K. Irreversibility Analysis in Hybrid Nanofluid Flow between Two Rotating Disks with Activation Energy and Cross-Diffusion Effects. *Chin. J. Phys.* **2021**, *72*, 499–529. [[CrossRef](#)]
17. Revathi, G.; Sajja, V.S.; Babu, M.J.; Raju, C.S.K.; Shehzad, S.A.; Bapanayya, C. Entropy optimization in hybrid radiative nanofluid (CH<sub>3</sub>OH + SiO<sub>2</sub> + Al<sub>2</sub>O<sub>3</sub>) flow by a curved stretching sheet with cross-diffusion effects. *Appl. Nanosci.* **2021**, 1–15. [[CrossRef](#)]
18. Alzahrani, H.A.H.; Alsaiari, A.; Madhukesh, J.K.; Kumar, R.N.; Prasanna, B.M. Effect of thermal radiation on heat transfer in plane wall jet flow of Casson nanofluid with suction subject to a slip boundary condition. *Waves Random Complex Media* **2022**, 1–18. [[CrossRef](#)]
19. Fetecau, C.; Shah, N.A.; Vieru, D. General solutions for hydromagnetic free convection flow over an infinite plate with Newtonian heating, mass diffusion and chemical reaction. *Commun. Theor. Phys.* **2017**, *68*, 768. [[CrossRef](#)]
20. Famakinwa, O.A.; Koriko, O.K.; Adegbe, K.S.; Omowaye, A.J. Effects of viscous variation, thermal radiation, and Arrhenius reaction: The case of MHD nanofluid flow containing gyrotactic microorganisms over a convectively heated surface. *Partial Differ. Equ. Appl. Math.* **2022**, *5*, 100232. [[CrossRef](#)]
21. Soundalgekar, V. Viscous dissipation effects on unsteady free convective flow past an infinite, vertical porous plate with constant suction. *Int. J. Heat Mass Transf.* **1972**, *15*, 1253–1261. [[CrossRef](#)]
22. Jusoh, R.; Nazar, R.; Pop, I. Magnetohydrodynamic boundary layer flow and heat transfer of nanofluids past a bidirectional exponential permeable stretching/shrinking sheet with viscous dissipation effect. *J. Heat Transf.* **2018**, *141*, 012406. [[CrossRef](#)]
23. Maleki, H.; Safaei, M.R.; Togun, H.; Dahari, M. Heat transfer and fluid flow of pseudo-plastic nanofluid over a moving permeable plate with viscous dissipation and heat absorption/generation. *J. Therm. Anal.* **2018**, *135*, 1643–1654. [[CrossRef](#)]
24. Kumar, K.A.; Sugunamma, V.; Sandeep, N. Influence of viscous dissipation on MHD flow of micropolar fluid over a slendering stretching surface with modified heat flux model. *J. Therm. Anal.* **2019**, *139*, 3661–3674. [[CrossRef](#)]
25. Afridi, M.; Qasim, M. Second law analysis of Blasius flow with nonlinear Rosseland thermal radiation in the presence of viscous dissipation. *Propuls. Power Res.* **2019**, *8*, 234–242. [[CrossRef](#)]
26. Ibrahim, W.; Tulu, A. Magnetohydrodynamic (MHD) boundary layer flow past a wedge with heat transfer and viscous effects of nanofluid embedded in porous media. *Math. Probl. Eng.* **2019**, *2019*, 1–12. [[CrossRef](#)]
27. Madhukesh, J.K.; Ramesh, G.K.; Roopa, G.S.; Prasannakumara, B.C.; Shah, N.A.; Yook, S.J. 3D Flow of Hybrid Nanomaterial through a Circular Cylinder: Saddle and Nodal Point Aspects. *Mathematics* **2022**, *10*, 1185. [[CrossRef](#)]
28. Dero, S.; Rohni, A.M.; Saaban, A. Effects of the viscous dissipation and chemical reaction on Casson nanofluid flow over the permeable stretching/shrinking sheet. *Heat Transf.* **2020**, *49*, 1736–1755. [[CrossRef](#)]
29. Mishra, A.K.; Pattnaik, P.K.; Mishra, S.R.; Senapati, N. Dissipative heat energy on Cu and Al<sub>2</sub>O<sub>3</sub> ethylene-glycol-based nanofluid flow over a heated semi-infinite vertical plate. *J. Therm. Anal.* **2020**, *145*, 129–137. [[CrossRef](#)]
30. Kumar, M.D.; Raju, C.S.K.; Sajjan, K.; El-Zahar, E.R.; Shah, N.A. Linear and quadratic convection on 3D flow with transpiration and hybrid nanoparticles. *Int. Commun. Heat Mass Transfer* **2022**, *134*, 105995. [[CrossRef](#)]

31. Gayatri, M.; Reddy, K.J.; Babu, M.J. Slip flow of Carreau fluid over a slendering stretching sheet with viscous dissipation and Joule heating. *SN Appl. Sci.* **2020**, *2*, 1–11. [[CrossRef](#)]
32. Chiranjeevi, B.; Valsamy, P.; Vidyasagar, G. Radiation absorption on MHD free convective laminar flow over a moving vertical porous plate, viscous dissipation and chemical reaction with suction under the influence of transverses magnetic field. *Mater. Today Proc.* **2020**, *42*, 1559–1569. [[CrossRef](#)]
33. Abbas, S.; Khan, M.I.; Kadry, S.; Khan, W.; Israr-Ur-Rehman, M.; Waqas, M. Fully developed entropy optimized second order velocity slip MHD nanofluid flow with activation energy. *Comput. Methods Programs Biomed.* **2020**, *190*, 105362. [[CrossRef](#)] [[PubMed](#)]
34. Gopal, D.; Saleem, S.; Jagadha, S.; Ahmad, F.; Almatroud, A.O.; Kishan, N. Numerical analysis of higher order chemical reaction on electrically MHD nanofluid under influence of viscous dissipation. *Alex. Eng. J.* **2020**, *60*, 1861–1871. [[CrossRef](#)]
35. Venkateswarlu, B.; Narayana, P.V.S. Cu-Al<sub>2</sub>O<sub>3</sub>/H<sub>2</sub>O hybrid nanofluid flow past a porous stretching sheet due to temperature-dependent viscosity and viscous dissipation. *Heat Transfer* **2021**, *50*, 432–449. [[CrossRef](#)]
36. Tassaddiq, A. Impact of Cattaneo-Christov heat flux model on MHD hybrid nano-micropolar fluid flow and heat transfer with viscous and joule dissipation effects. *Sci. Rep.* **2021**, *11*, 67. [[CrossRef](#)]
37. Khan, M.I.; Hafeez, M.U.; Hayat, T.; Khan, M.I.; Alsaedi, A. Magneto rotating flow of hybrid nanofluid with entropy generation. *Comput. Methods Programs Biomed.* **2020**, *183*, 105093. [[CrossRef](#)]
38. Ramesh, G.; Madhukesh, J.; Das, R.; Shah, N.A.; Yook, S.-J. Thermodynamic activity of a ternary nanofluid flow passing through a permeable slipped surface with heat source and sink. *Waves Random Complex Media* **2022**, 1–21. [[CrossRef](#)]
39. Shah, N.A.; Yook, S.-J.; Tosin, O. Analytic simulation of thermophoretic second grade fluid flow past a vertical surface with variable fluid characteristics and convective heating. *Sci. Rep.* **2022**, *12*, 5445. [[CrossRef](#)]
40. Acharya, N.; Mabood, F. On the hydrothermal features of radiative Fe<sub>3</sub>O<sub>4</sub>-graphene hybrid nanofluid flow over a slippery bended surface with heat source/sink. *J. Therm. Anal.* **2020**, *143*, 1273–1289. [[CrossRef](#)]
41. Zainal, N.A.; Nazar, R.; Naganthran, K.; Pop, I. Stability analysis of MHD hybrid nanofluid flow over a stretching/shrinking sheet with quadratic velocity. *Alex. Eng. J.* **2020**, *60*, 915–926. [[CrossRef](#)]
42. Gul, T.; Bilal, M.; Alghamdi, W.; Asjad, M.I.; Abdeljawad, T. Hybrid nanofluid flow within the conical gap between the cone and the surface of a rotating disk. *Sci. Rep.* **2021**, *11*, 1180. [[CrossRef](#)] [[PubMed](#)]
43. Wang, J.; Xu, Y.-P.; Qahiti, R.; Jafaryar, M.; Alazwari, M.A.; Abu-Hamdeh, N.H.; Issakhov, A.; Selim, M.M. Simulation of hybrid nanofluid flow within a microchannel heat sink considering porous media analyzing CPU stability. *J. Pet. Sci. Eng.* **2021**, *208*, 109734. [[CrossRef](#)]
44. Gul, H.; Ramzan, M.; Nisar, K.S.; Mohamed, R.N.; Ghazwani, H.A.S. Performance-based comparison of Yamada–Ota and Hamilton–Crosser hybrid nanofluid flow models with magnetic dipole impact past a stretched surface. *Sci. Rep.* **2022**, *12*, 29. [[CrossRef](#)]
45. Gumber, P.; Yaseen, M.; Rawat, S.K.; Kumar, M. Heat transfer in micropolar hybrid nanofluid flow past a vertical plate in the presence of thermal radiation and suction/injection effects. *Partial Differ. Equ. Appl. Math.* **2021**, *5*, 100240. [[CrossRef](#)]
46. Abbas, Z.; Naveed, M.; Sajid, M. Hydromagnetic slip flow of nanofluid over a curved stretching surface with heat generation and thermal radiation. *J. Mol. Liq.* **2016**, *215*, 756–762. [[CrossRef](#)]
47. Dawar, A.; Wakif, A.; Thumma, T.; Shah, N.A. Towards a new MHD non-homogeneous convective nanofluid flow model for simulating a rotating inclined thin layer of sodium alginate-based Iron oxide exposed to incident solar energy. *Int. Commun. Heat Mass Transf.* **2021**, *130*, 105800. [[CrossRef](#)]
48. Waini, I.; Ishak, A.; Pop, I. Hybrid Nanofluid Flow Past a Permeable Moving Thin Needle. *Mathematics* **2020**, *8*, 612. [[CrossRef](#)]
49. Mukhopadhyay, S. Effect of thermal radiation on unsteady mixed convection flow and heat transfer over a porous stretching surface in porous medium. *Int. J. Heat Mass Transf.* **2009**, *52*, 3261–3265. [[CrossRef](#)]